Analysis of diamond wheel wear and surface integrity in laser-assisted grinding of RB-SiC ceramics

Xiaoshuang Rao[a,b], Feihu Zhang[a], Yanjun Lu[c], Xichun Luo[b*],Fei Ding[b], Chen Li [a*]

[a] *School of Mechatronics Engineering, Harbin Institute of Technology, Harbin 150001, China*

[b] *Centre for Precision Manufacturing, DMEM, University of Strathclyde, Glasgow G1 1XQ, UK*

[c] *Guangdong Provincial Key Laboratory of Micro/Nano Optomechatronics Engineering, College of Mechatronics and Control Engineering, Shenzhen University, Shenzhen 518060, China*

*Corresponding author E-mail address: *xichun.luo@strath.ac.uk, *hit_chenli@163.com*

Abstract: Laser-assisted grinding provides a promising solution for achieving cost-efficient machining of hard and brittle materials. However, the heat generated by laser may cause the wear of diamond grinding wheel, including the wear of both diamond grits and bond material. Consequently, wheel wear has a knock-on effect on the ground surface roughness. Moreover, the laser irritation may also induce damage in the machined surface. This paper focuses on the investigation of wear of diamond grinding wheel and surface integrity in laser-assisted grinding of RB-SiC ceramics. Different temperatures were obtained by setting the laser power to explore the influence of heat on wheel wear and surface integrity. The wear modes and mechanism of the diamond grits and bond material were analyzed by combination of SEM detection and energy dispersion spectrum analysis. The results revealed that adhesion and pullout of diamond grits in laser-assisted grinding were the remarkable difference from those in

conventional grinding due to the thermal softening of both RB-SiC specimen and bond material of the grinding wheel. Surface roughness was then improved owing to the increase in active grits. The Raman spectra of the machined surface also revealed different stress conditions and microstructures of the Si and SiC Phase in RB-SiC ceramics. These results provided insight on quality control in laser-assisted machining of RB-SiC ceramics.

Keywords: Laser-assisted grinding; grinding wheel wear; surface integrity; high temperatures

1 Introduction

Reaction-bonded silicon carbide (RB-SiC) ceramic is typical difficult-to-machine material because of its high hardness and brittleness, which indicates low material removal rate and serious tool wear. Laser-assisted machining is regarded as a promising method for cost-effective machining of ceramic materials as its advantage in reduction of material strength and increase of machinability [1–3]. However, the softened material induce by a focused laser beam with highly intense thermal energy will result in the changes of material removal mode as well as the cutting tool-workpiece interaction during the process [4]. The increase in visco-plastic flow induced by heat enables the ductile material removal and adhesion of the tool [5]. Thereby, laser-assisted machining process, as to conventional machining process, will make remarkable difference on the tool wear mechanisms and the machined surface integrity.

The tool wear is always a research hotspot due to its direct association with the machined surface quality. In grinding of hardened AISI 52100 bearing steel, the wheel

dressing and wear effects were proved to be the most influential factors for ground surface roughness [6]. Lower surface roughness was obtained as the grinding wheel surface was in a good dressing condition [7]. The patterns of grinding wheel wear transferred to the workpiece surface contributed to the tool-dependence of the final surface finish [8]. Therefore, the grain protrusion topography [9], active grits count [10], distribution and shape of the cutting edges [11], and even the whole grinding wheel topography [12] have been investigated in order to understand and control the influence of wheel wear on surface roughness. Different models were then proposed to evaluate and predict the wheel wear based on the wheel-workpiece contact area [8,13,14]. However, the wheel wear characteristics is not only influenced by the tool-workpiece interaction but also determined by the workpiece temperature [5], especially in the laser-assisted machining process.

Actually, thermal assistance has been reported to have different effects on machinability of structure ceramics, superalloys and metals, including specific cutting energy, tool wear rate, surface roughness, material removal rate, and surface integrity [15]. The tool damage was reported to be reduced in laser-assisted machining [16,17]. Due to the decrease in material strength at higher temperature, the tool flank wear decreased with the increase of workpiece temperature in laser-assisted turning of silicon nitride ceramics [5]. On the other hand, an excessive temperature was also found with an adverse influence on flank wear because of the reduction in tool strength [1]. The optimum temperature was then investigated and confirmed in existence for improving tool life [2,18]. Moreover, the previous researches on tool wear were only focused on

the turning and milling processes with laser assistance. However, the grinding wheel wear characteristic, especially for grinding wheel with diamond grits, and its influence on surface roughness are largely absence in the study of laser-assisted machining process. Different from the tool with one or limited cutting edges in turning or milling process, the grinding wheel is composed of abundant cutting edges fasten on the surface of metal matrix by bond material. The heat on workpiece surface generated by focused laser is transferred to the grinding wheel during the process, changing the work behavior of grinding wheel, like the effective hardness of grinding layer [19]. Moreover, excessive heat may also cause the thermal damage of diamond grits as the diamond has a low thermal stable temperature in atmosphere [20].

Therefore, the wear of diamond grinding wheel, including diamond grits and bond material, is fully analyzed in laser-assisted grinding of RB-SiC ceramics in present work. The wear modes of diamond grits are discussed in detail under different temperatures realized by varied laser powers. Machined surface roughness is then investigated based on the wear of diamond grinding wheel. Besides, the surface damages induced by laser heat, such as residual stress and phase transformation, are also evaluated by Raman spectra.

2 Experimental details

2.1 Material and tool

RB-SiC ceramic off ered by Goodfellow Cambridge Ltd. (UK) was cut into specimen in dimensions of 10 mm×10 mm×6 mm by wire electrical discharge machining. The amount of remnant Si in the RB-SiC ceramic is 10% in volume. Five electroplated

diamond wheels with grain size of 64 μm and 100% concentration were used in the machining tests. Figure 1 (a) shows the original surface morphology of the electroplated diamond wheel before the machining tests. The result of energy dispersion spectrum (EDS) obtained at the region "A" in Fig. 1 (a) reveals the constituent of Ni element, which composes of the electroplated bond material, as shown in Fig. 1 (b).

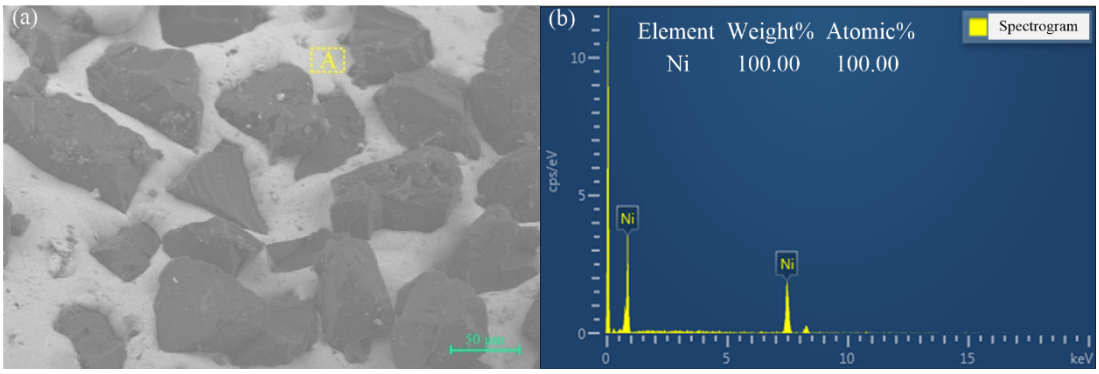

Fig. 1 Surface morphology and energy dispersion spectrum of the electroplated diamond wheel. (a) The original surface morphology before the machining trails; (b) the EDS result of the electroplated bond material.

2.2 Experimental setup

The experiment was conducted on an ultra-precision machine-micro-3D, as shown in Fig. 2. A clamp spring was used to connect the electroplated diamond wheel with the spindle. RB-SiC specimen was fixed in the sink of the insulating asbestine block by the bench vice mounted on a dynamometer. The dynamometer was then installed on the worktable. To obtain uniform machined surface before the grinding test was performed, all specimens were flatted at feed rate of 10 mm/min, cutting depth of 2 μm and spindle speed of 8000 r/min.

A fibre laser with maximum power of 200 W was used to heat the specimen during the machining process. To investigate the influence of temperatures on the diamond wheel

wear, machined surface roughness, and surface damage, the laser powers of 20 W, 40 W, 80 W and 160W were selected to produce corresponding temperatures of 200 ℃, 600 ℃, 900 ℃ and 1200 ℃ on the machined surface of RB-SiC specimens. In our previous work [21], the desired temperatures were investigated to find that they could only be obtained after a special preheating period under different laser powers. Therefore, all specimens were heated enough time before the laser-assisted grinding tests were performed. Simultaneously, a contrast grinding test was also conducted at room temperature (RT, 23.7 ℃). The details of the experimental conditions are listed in Table 1.

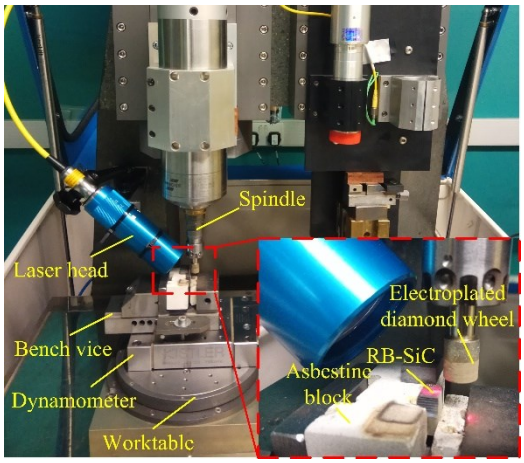

Fig. 2 Experimental setup of the laser-assisted grinding

Table 1 Experimental conditions

Parameters	Values
Grinding wheel	Electroplated, 6 mm in diameter and 12 mm in width, grit size of 64 μm
Workpiece material	RB-SiC (10% free Si)
Resultant temperature (℃)	RT, 200, 600, 900, 1200
Coolant	Without (dry grinding)

Spindle speed (rmp)	8000
Feed rate (mm/min)	10
Depth of cut (μm)	10

2.3 Characterization and measurements

To characterize wheel wear and machined surface, all electroplated diamond wheels and specimens were ultrasonically cleaned for 10 min in acetone after the grinding tests. Their morphologies were then detected by scanning electron microscopy (SEM, Merlin Compact). The EDS technique was used to check the element contents on the surfaces of the diamond grit and bond material after grinding tests. The machined surface roughness (S_a) was measured by a white light interferometer (Zygo cp-200) at eight different locations and then took the average as the roughness results. The machined surface/subsurface damage was detected by a Raman system (inVia-Reflex).

3 Results and discussion

3.1 The wear of electroplated diamond wheel

The wheel wear is both an important factor affecting the machined surface roughness [17] and a metric to evaluate the tool life. This part focuses on the wheel wear by a combination of the wheel topography observation and EDS analysis. Different wear modes of diamond grits and bond material will be paid much attention at different resultant temperatures.

3.1.1 Surface topography of electroplated diamond wheel after grinding tests

Figure 3 shows the surface topographies of the electroplated diamond grinding wheel after grinding tests at different temperatures. It reveals the different wear topographies

of diamond grits at different temperatures. When the test was conducted at room temperature, the diamond grits were characterized with flat and fracture, as shown in Fig. 3 (a). This is attributed to few grits in grinding because of the grit distribution with high protrusion on the grinding wheel surface, which will be discussed in detail in Section 3.2.2. However, more grit wear modes besides flat and fracture, such as adhesion and pullout, are found in laser-assisted grinding shown in Fig. 3 (b) ~ (e). Moreover, the adhesion tends to increase with the increase of temperatures. During the laser-assisted machining, the workpiece material was suggested to soften at high temperature and adhere to the cutting tool [5]. As a result, adhesion easily occurs when the ascending temperature increases the material softening. In addition, the worn flat of diamond grits gradually disappears as the temperature increases, as shown in Fig.3 (d) and (e). It indicates the adhesion prevents the grits from worn flat because of the material softening, which may be conducive to prevent the wear of diamond grits and prolong the wheel life [2,19].

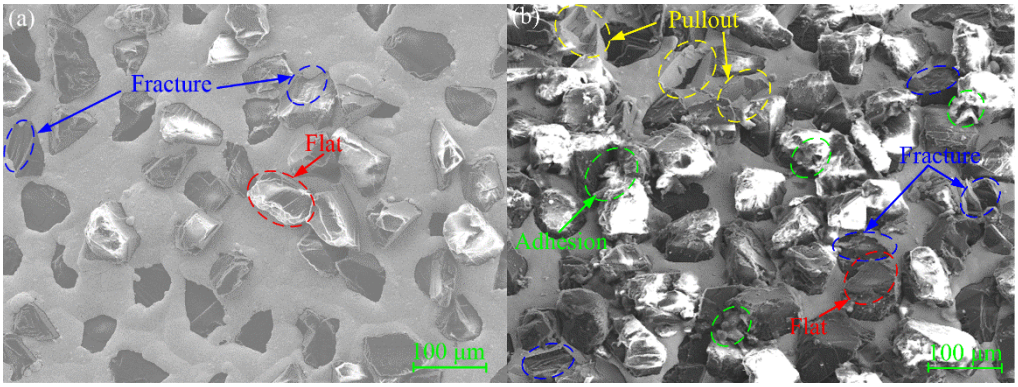

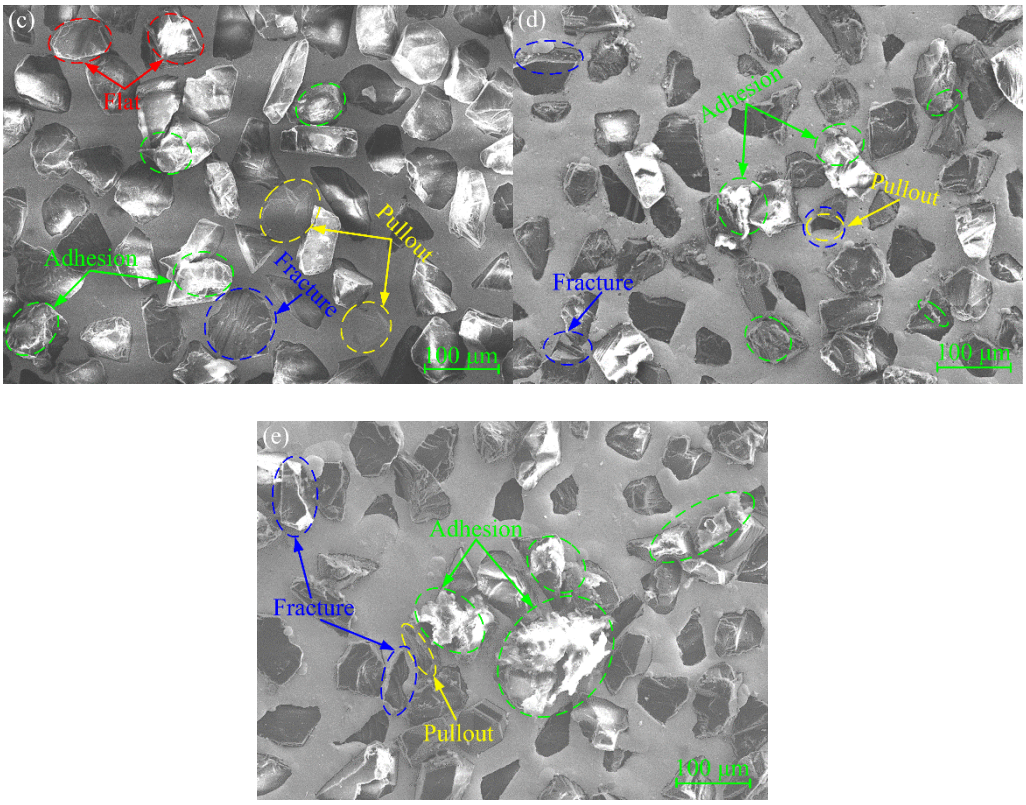

Fig. 3 Surface morphologies of electroplated diamond wheel at different temperatures after grinding tests. (a) RT, (b) 200 ℃, (c) 600 ℃, (d) 900 ℃ and (e) 1200℃.

In addition, another typical wear characteristic of diamond grit was the pullout in laser-assisted grinding tests. The heat induced by the laser irritation on the material surface was transferred to the grinding wheel through the contact between the grinding wheel and RB-SiC specimen. As a result, the strength of bond material decreases. The diamond grits were then pulled out at high resultant force and pits were left on the wheel surface. Therefore, the wear mode of bond material can be determined through the EDS analysis, which will be detailly discussed in Section 3.1.3.

3.1.2 Adhesion of diamond grit

To further determine the adhesive wear mode in the laser-assisted test, data of elements were collected by line scan across the diamond grit and bond material using EDS

technology, as shown in Fig. 4. The spectrums of C and Ni elements, as predicted, appears a peak on the diamond grit surface and the bond material surface, respectively. No Si content is discovered on the surface of the diamond grit with worn flat mode in grinding test at room temperature. However, the Si contents are detected on and/or around the diamond grits in laser-assisted grinding tests at all temperatures, seeing Fig. 4 (b) ~ (e). This implies that all adhesion occurred in laser-assisted grinding is mainly attributed to the remnant Si softening in RB-SiC ceramics. Relative to SiC phase, the lower melting point of Si phase (1410 ℃) [22] makes it be easily softened and adhere to the diamond grit with the help of visco-plastic flow at high temperatures. Moreover, the oxide content is also detected in a same varied tendency alike that of the Si spectrum, which indicates the Si adhered on/around the grits is oxidized at high temperatures.

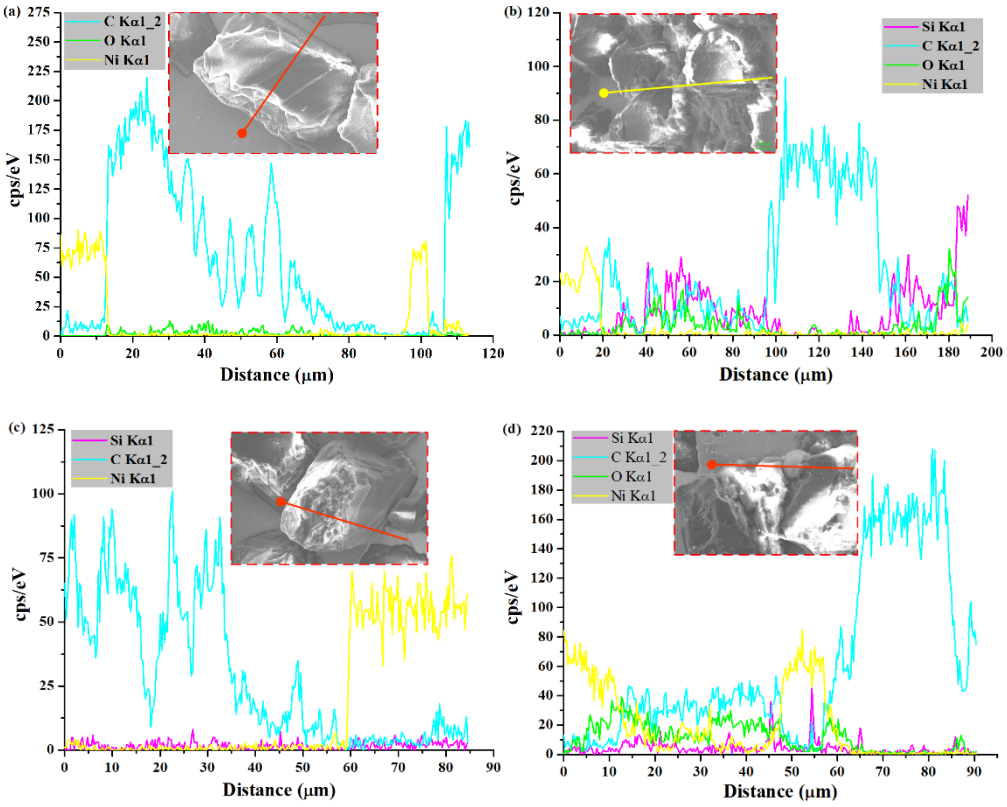

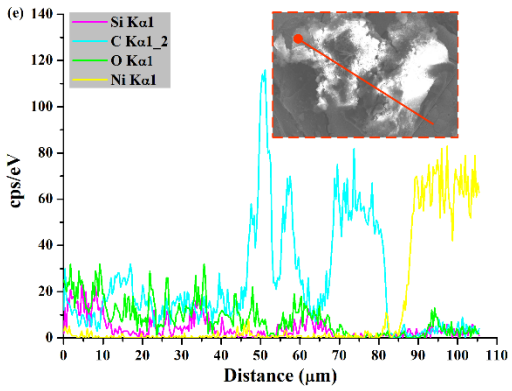

Fig. 4 EDS analysis of the adhesion of the diamond grit at different temperatures in grinding test. (a) RT, (b) 200 ℃, (c) 600 ℃, (d) 900 ℃ and (e) 1200℃.

3.1.3 Wear of bond material

As mentioned above, the wear of bond material can be determined by analysis of the grit pullout. At different temperatures, the pullouts of diamond grits on the surface of grinding wheel were detected by SEM and shown in Fig. 5. The diamond grit is pulled out from the bond material of the grinding wheel when its strength is not enough to hold the grit under the grinding force [23,24]. Therefore, the variation of the bond strength can be derived from the topography of diamond grit pullout combined with the EDS analysis. As the high-level spectrum of C element is detected in the pit shown in Fig. 5 (a), the pullout of diamond grit can be identified as resulting from the grit large-scale fracture at room temperature. However, the spectrums of C and Ni elements appear peaks in different remained pits at 200 ℃, as shown in Fig. 5 (b). Fewer C contents detected in the left pit indicates that the grit with shallow penetration depth is fully pulled out, while high C contents detected in the right pit reveals that the grit pullout results from large-scale fracture. Furthermore, no C contents are detected in the remained pits when the resultant temperatures in RB-SiC specimen further increase, as

shown in Fig 5 (c) ~ (d). It indicates that higher temperature results in the full pullout of diamond grit on wheel surface. Simultaneously, it should be note that the remained pits on the wheel surface at higher temperatures are deeper than that at 200 ℃, which means that the grits deeper embedded in the nickel bond are also pulled out at higher temperatures. This is because the amount of thermal transmission to diamond wheel increases by contacting with the RB-SiC specimen due to the resultant temperature ascends. The strength of bond material is then degraded because of the softening effect. The holding force of bond material is consequently reduced to loss the grits. The temperature is higher, the holding force is lower. As a result, deeper remained pits are formed as the grit is fully pulled out.

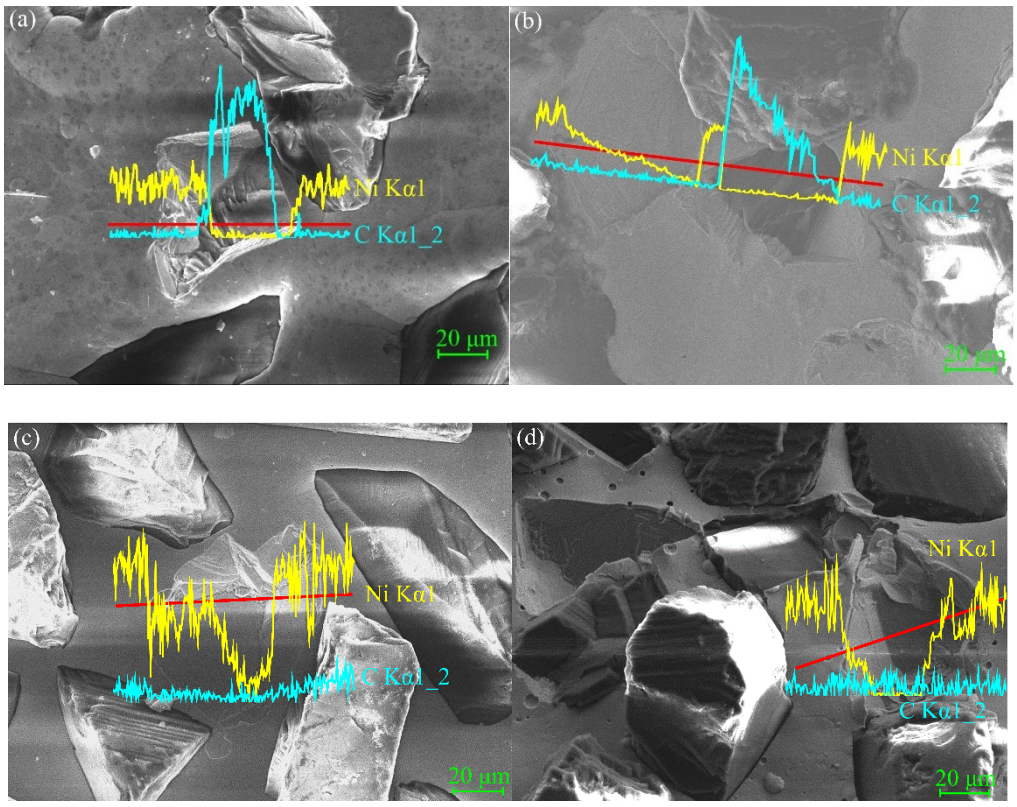

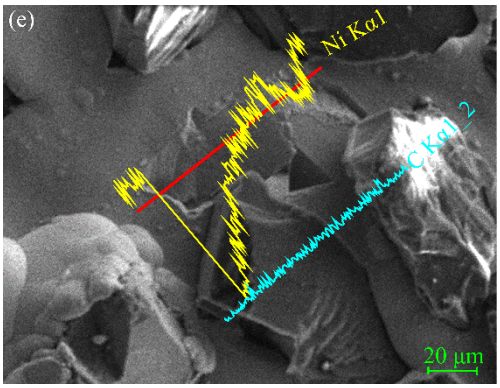

Fig. 5 Pullout of grits and EDS analysis in grinding tests at different temperatures. (a) RT, (b) 200 ℃, (c) 600 ℃, (d) 900 ℃ and (e) 1200℃.

3.2 Machined surface integrity

In the previous work [21,25], the influences of temperatures on the mechanical property and material removal mode of RB-SiC ceramics had been investigated by indentation and scratching tests. The results revealed the heat facilitated the reduction in hardness and improvement of ductile material removal at elevated temperatures. As a result, the machined surface differs somewhat in surface morphology, waviness, roughness, and phases transition at elevated temperatures. In this section, the machined surface integrity has been explained by the wheel wear as well as the heat effect at different temperatures.

3.2.1 Machined surface morphology

Fig. 6 shows the machined surface morphology of RB-SiC ceramics ground at different temperatures. It is obvious that fracture is the main characteristic for all machined surface due to RB-SiC ceramic is mainly removed in brittle regime. However, some ductile grinding tracks (marked by arrows in the figures) are also detected on the machined surface, which is attributed to the varied grit protrusion with shallower actual

depth of cut. The ductile material removal mode can be obtained as the actual depth of cut is less than the critical depth of cut given by [26]:

$$d_c = 0.15\left(\frac{E}{H}\right)\left(\frac{K_c}{H}\right)^2 \quad (1)$$

Where E, H, and K_C are the elastic modulus, hardness, and fracture toughness of the material at room temperature, respectively. However, Eq. (1) has been modified by considering the variation of mechanical property at elevated temperatures in the previous work [25], which is given by:

$$d_c = 0.52\left(\frac{E}{H}\right)\left(\frac{K_c}{H}\right)^2 \quad (2)$$

Eq. (2) indicates the critical depth of cut increase at elevated temperatures. As a result, more active grits on the surface of the grinding wheel will interact with the RB-SiC specimen with a deeper actual depth of cut in ductile material removal regime. Consequently, more ductile grinding tracks are detected on the machined surfaces at elevated temperatures, as shown in Fig. 6 (b)~(e). Furthermore, the ductile area composed by the ductile grinding tracks tends to increase as the temperature increases.

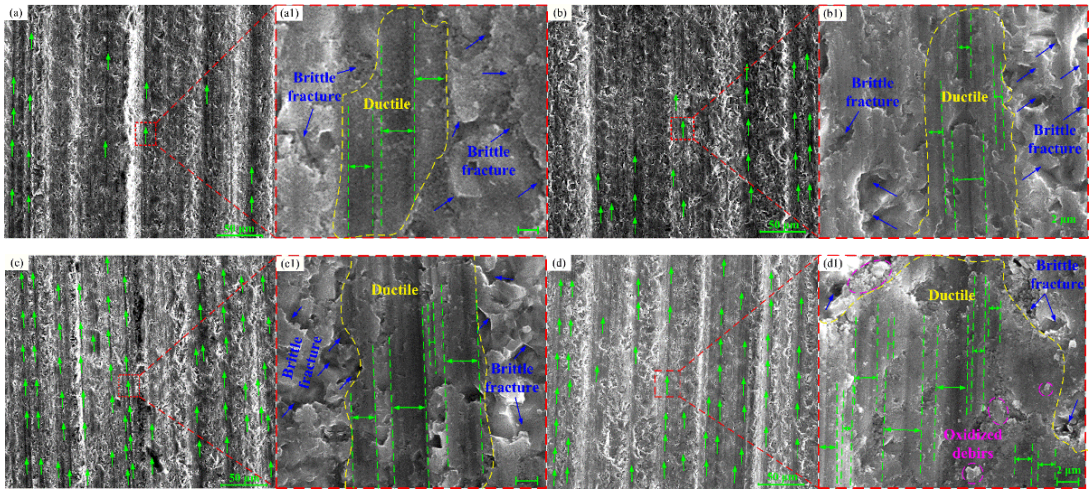

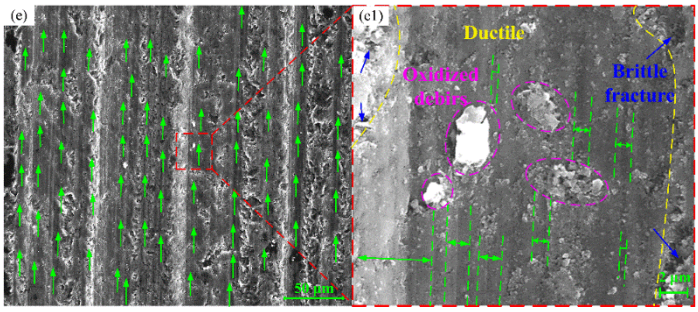

Fig. 6 SEM micrographs of the machined surface ground at different temperatures. (a) RT, (b) 200 ℃, (c) 600 ℃, (d) 900 ℃ and (e) 1200℃.

In addition, the ductile grinding tracks are shown by magnifying the ductile area, seeing in Fig.6 (a1) ~ (e1). The grinding tracks are characterized with broad width at room temperature. Less ductile grinding tracks are found in the ductile area. However, the amounts of the grinding track tend to increase when the temperature increases. At higher temperatures, the interfered phenomenon even occurs among the tracks so that a flat ductile surface is formed in the ductile area, as shown in Fig 6 (e1). It indicates that the active grits increase in grinding of RB-SiC ceramics at elevated temperature. This is attributed to a normal distribution of grit protrusion height on wheel surface [12], which will be discussed in detail in Section 3.2.2. Moreover, due to adhesion and friction between diamond grits in wheel and RB-SiC specimen at higher temperatures, oxidized debris is found on the ground surface of the ductile area, as shown in Fig 6 (d1) and (e1).

3.2.2 Machined surface roughness

The surface roughness was measured by white light interferometer. A 3D surface morphology was then obtained, as shown in Fig. 7. More detail characteristics of machined surface, including ridge and gully, are presented by the simulated topography.

Both ridge and gully of the machined surface topography increases in their numbers as the temperature increases. The cross-sectional profile shown at the bottom of the Fig.7 indicates that the surface waviness tends to be regular and periodic, showing more symmetric about the centerline as the temperature increases. Furthermore, the height of the ridge or the depth of the gully also decreases with the increase in temperatures. As a result, the surface roughness will decrease as its arithmetic mean value, S_a, is generally defined as [27]

$$S_a = \frac{1}{l_x l_y} \iint_S |\eta(x, y)| dxdy \tag{3}$$

Where l_x, l_y are the evaluation lengths of the measured surface in the x and y directions, $\eta(x,y)$ is the distance of the measurement point on the surface profile from the measurement center-plane (S). The surface roughness is then obtained at different temperatures, shown in Fig. 8. It is obvious that the surface roughness decreases as the temperature increases. The surface roughness of 1.37 μm at 1200 ℃ decreases by 41.2 % against 2.33 μm at room temperature. The error bar of surface roughness calculated by eight roughness measurements has also shorten with the increase in temperatures. It further indicates that smoother surface is achieved in laser-assisted grinding because of the enhancement in ductile material removal.

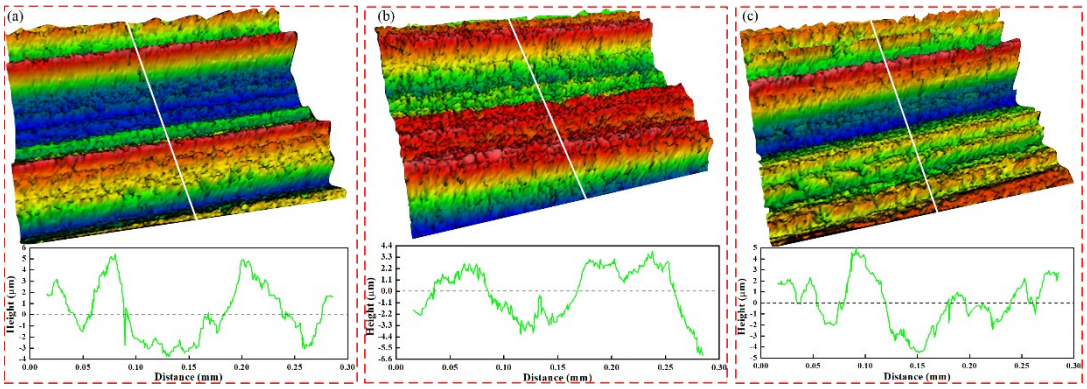

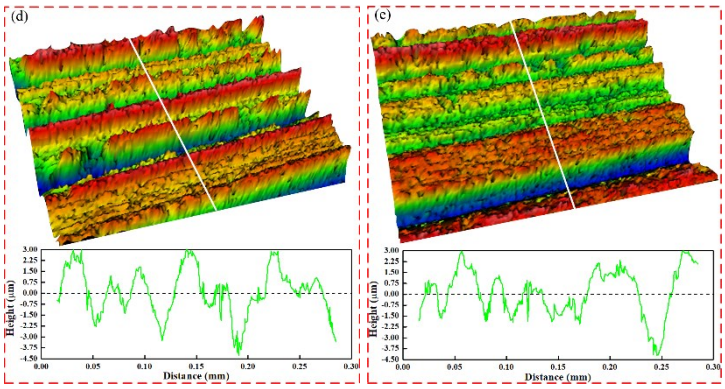

Fig.7 3D surface topography measured by white light interferometer for RB-SiC ceramics ground at elevated temperatures. (a) RT, (b) 200 ℃, (c) 600 ℃, (d) 900 ℃ and (e) 1200℃.

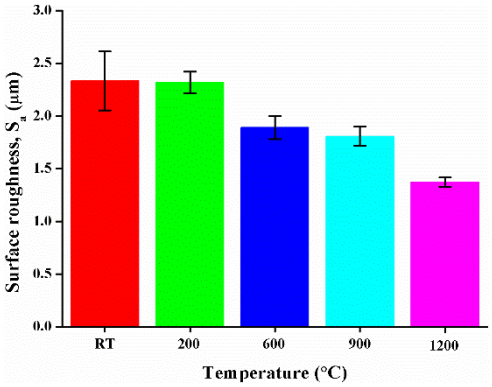

Fig.8 Surface roughness in laser-assisted grinding of RB-SiC ceramics at different temperatures.

The distribution of the diamond grit protrusion on the surface of grinding wheel may contribute to the decrease in surface roughness at elevated temperatures, as shown in Fig. 9. Darafon et al. [12] and Setti et al. [10] studied on the distribution of the different protrusion heights of grits, and the results revealed a normal distribution between the maximum and minimum values. It implies that the most grits protrude the surface of grinding wheel with the mean height while few grits protrude with maximum or minimum height. Therefore, only few grits with maximum protrusion height take part

in grinding of RB-SiC ceramics at room temperature according to the wear morphology of grinding wheel shown in Fig. 3 (a). The actual depth of cut is only dependent on the maximum protruded grits (such as the grit 1 in Fig. 9) and roughly equal to the given value (d1 ≈ 10 μm). As a result, a rough surface with broad and deep valley of cross-sectional profile will be formed, seeing the surface cross-sectional profile 1 in Fig. 9. The machined surface topography shown in Fig. 7 (a) and higher surface roughness shown in Fig. 8 at room temperature are then obtained.

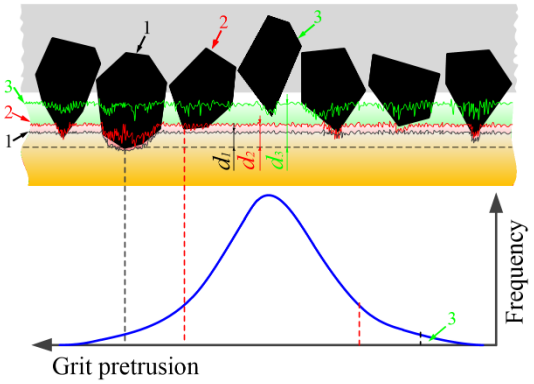

Fig. 9 Schematic of diamond grits on surface of electroplated grinding wheel and the probability distribution of grit protrusion.

However, the actual depth of cut (d_2) increases due to thermal expansion of workpiece material caused by laser-heating [28]. As a result, the grits with mean protrusion height, such as the grit 2 in Fig. 9, will also take part in grinding. The narrowed space between two adjacent grits makes a cross-sectional profile of machined surface with a gradually shorten distance between peak and valley, as shown in Fig. 7 (b)~(e). Simultaneously, the deepened actual depth of cut increases the grinding force of diamond grits, as shown in Fig. 10. The thermal expansion of RB-SiC specimen at elevated temperatures is responsible for the increase in actual depth of cut and then leads to the increase in

grinding force. Furthermore, the holding force of bond material for grinding wheel will decrease due to thermal softening [29]. Therefore, the maximum protruded grit 1 will be pulled out when the grinding force further increase and the holding force of bond material decrease at higher temperatures. The grit 3 with the minimum protrusion height also penetrates machined surface at further thermal expansion. The interference occurred in the tracks of diamond grits produces the surface profile 3. Eventually, a low surface roughness is obtained at higher temperatures.

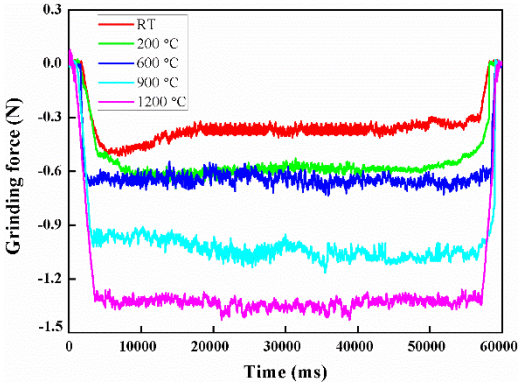

Fig. 10 Cutting force at different temperature.

3.2.3 Machined surface/subsurface damages

The surface/subsurface damage, such as residual stress [30,31], phase transformation [32,33], disorder and stacking faults [34] can be characterized by Raman spectroscopy through the Raman parameters as bandwidth, intensity, frequency shift and polarization properties of the Raman bands [35]. Therefore, the machined surface of RB-SiC ceramics ground at different temperatures was irradiated by the Raman laser beams (325 nm) with a laser power of 20 mW. The Raman spectrums are depicted in Fig. 11. Fig. 11 (a) shows the whole Raman spectra of RB-SiC ceramics in the range of 0-1800 cm^{-1} at different temperatures. The folded modes of transverse acoustic (FTA) at 150.1

and 241.0 cm^{-1}, the folded modes of transverse optic (FTO) at 765.5, 787.1 and 796.0 cm^{-1}, and the folded modes of longitudinal optic (FLO) at 964.4 cm^{-1} are identified as the 6H-SiC phase referenced to the literature [36]. While the longitudinal optic (LO) of Raman peak at 522.1 cm^{-1} is identified as the crystalline Si. Moreover, the FTO mode at 796.0 cm^{-1} is also ascribed to 3C-SiC polytype [34,36]. As a result, the RB-SiC ceramic has been proved to consist of 6H-SiC, 3C-SiC and Si phases. However, to identify the damage induced by the laser-assisted grinding, more detail analysis needs to be conducted at the Raman peaks, as shown in Fig.11 (a1) ~(a3).

The Raman spectra of Si exhibit a single peak at all temperatures, seeing Fig. 11 (a1). Obviously, the peak of Raman spectra occurs at the frequency of 522.1 cm^{-1} on the initial surface and the surface ground at room temperature and 200 ℃, which are positive shift compared to the standard Raman spectrum of Si at 520 cm^{-1}. According to reference [30,31], there is a relationship between the Raman shift and residual stress given by

$$\sigma = -435\Delta w \tag{4}$$

Where σ is the residual stress and Δw is the strain-induced shift of the Raman frequency. Eq. (4) indicates compressive stress existed in the free Si of RB-SiC ceramics on the initial surface and the surface ground at room temperature and 200 ℃. However, the spectra shift to 520.7 cm^{-1}, which is very closed to the standard spectrum peak of the silicon substrate at 520 cm^{-1}. It indicates that the compressive stress of Si phase is released because of larger visco-plastic flow at higher temperature. Moreover, the gradually broaden band of Raman spectra with increase in temperature also

indicates amorphous phase [37] occurred in laser-assisted grinding.

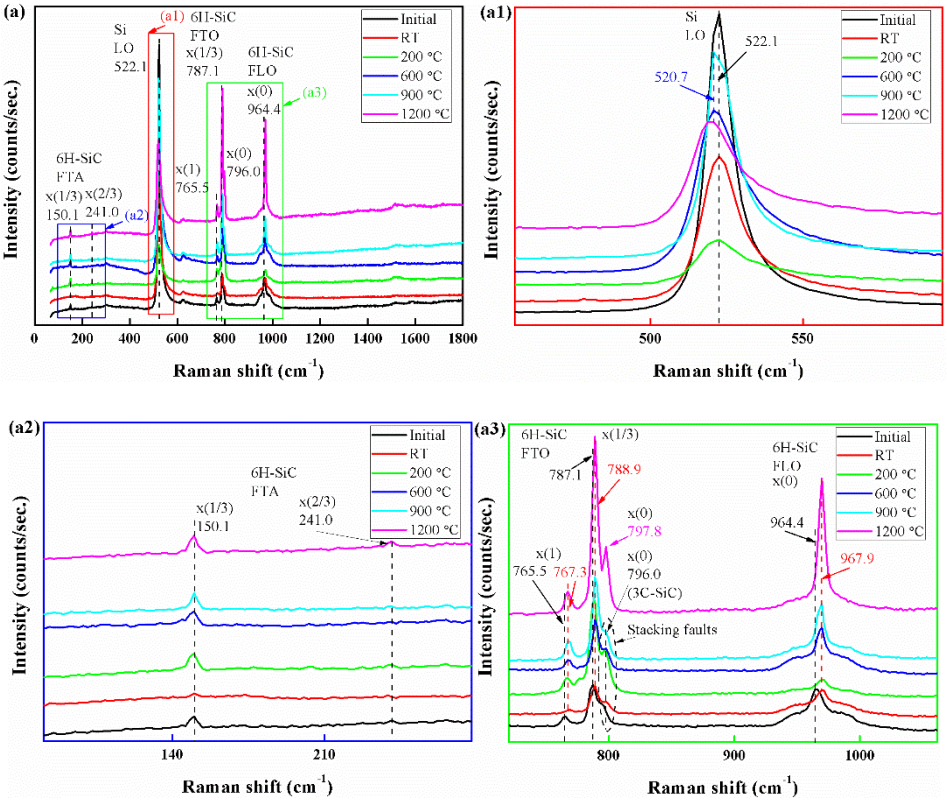

Fig. 11 Results of the Raman spectra. (a) Raman spectra of RB-SiC ceramics ground at different temperature, (b) local magnification spectra of Si, (c) and (d) local magnification spectra of 6H-SiC in different ranges.

In addition, the Raman spectra of 6H-SiC are depicted in Fig. 11 (a2) and (a3). Though no significant differences in Raman spectra are found at elevated temperature as comparing to the Raman spectrum obtained in pristine RB-SiC for the FTA mode at 150.1 and 241.0 cm^{-1}, all Raman spectra of 6H-SiC shift to higher frequencies for FTO and FLO modes in grinding tests. It indicates further compressive stress occurred in 6H-SiC phase at room and elevated temperatures. As stacking faults accompanying partial dislocations make the phonon lifetime and contribute to the broadening of the phonon Raman bands [35], the gradually narrowed frequency bands of FTO and FLO

modes suggests the increase in the generation of 6H-SiC phase. Matsunami et al [32] pointed out that 6H-SiC can be grown on 3C-SiC substrates by temperature and applying rearranged surface to crystal growth. Therefore, due to the intensity increases and the Raman band becomes narrow as the increase in temperature, the stacking faults around the frequency of 796.0 cm^{-1} (the aforementioned Raman peak of 3C-SiC) and disorder phase around the frequency of 964.4 cm^{-1} can be deemed to transform to or generate 6H-SiC phase as the crystal surface atomic rearrangement at high pressure (compressive) and temperature.

4 Conclusion

In this paper, diamond grinding wheel wear and machined surface integrity have been investigated in laser-assisted grinding. The wear of diamond grits and bond material are analyzed in detail under different processing temperatures. In consideration the influence of wheel wear and heat on the surface integrity, the machined surface morphology, roughness and damage have also been characterized. The following conclusions can be drawn:

(1) The diamond grinding wheel shows different wear morphology at different processing temperatures in laser-assisted grinding. Different from the wear modes of fracture and flat at room temperature, the diamond grits show more wear modes of adhesion and pullout at elevated temperatures due to the thermal transmission. The adhesion plays an important role in laser-assisted grinding of RB-SiC as it prevents diamond grits from wear flat, which may prolong the wheel life.

(2) The analysis of grit adhesion mode by EDS shows adhesion occurred at elevated

temperatures is attributed to the free Si softening. At high temperature, the adhesive Si on the diamond is found to be oxidized in air.

(3) The pullout of diamond grits on the surface of grinding wheel can indicate the bond strength in laser-assisted grinding process. Compared to that occurred at the room temperature which is attributed to grits fracture, the pullout of diamond grits at elevated temperature is attributed to strength degradation of bond material induced by thermal transmission. As a result, the diamond grits with deeper penetrations are fully pulled out due to the holding force of bond material decreases, which is benefit for grinding performance of diamond wheel.

(4) The machined surface morphology shows an ascending tendency of forming ductile grinding tracks with the increase in temperatures, which is attributed to the increase in critical depth of cut due to the varied mechanical properties at elevated temperature. As a result, more active grits remove the material in ductile regime. It illustrates that laser-assisted grinding can improve surface finish by promoting ductile material removal.

(5) As grits with maximum protrusion height were pulled out by high cutting force and thermal expansion of RB-SiC specimens induced by laser heating, machined surface topography is characterized by more ridges and gullies with lower height and depth at elevated temperature. The machined surface waviness also becomes more regular and periodic at high temperatures comparing to that at room temperature. Consequently, the surface roughness decreases with the increase in temperatures. The maximum reduction in surface roughness is at 1200 ℃by 41.2 %

as compared to that at room temperature.

(6) Analysis on the machined surface using Raman spectroscopy shows compressive stress occurred in initial surface and ground surface at room temperature and 200 ℃ while almost stress free at higher temperatures for Si phase. It indicates that larger visco-plastic flow releases the compressive stress in Si phase. The Raman spectra shift and its narrowed bandwidth of 6H-SiC phase indicates stacking faults and disorder phase transform to or generate new 6H-SiC phase as the crystal surface atomic will be rearranged at high pressure (compressive) and temperature.

Data Statement

All data underpinning this publication are openly available from the University of Strathclyde KnowledgeBase. https://doi.org/10.15129/db923c2f-9cec-47d5-a1d2-9540dea366e4

Acknowledgements

This work was supported by the National Science and Technology Major Project of China (2018ZX04015001-005). The authors also gratefully acknowledge the financial support from the EPSRC (UK) (EP/K018345/1) and National Natural Science Foundation of China (51805334) for this study.

References:

[1] P.A. Rebro, Y.C. Shin, F.P. Incropera, Laser-Assisted Machining of Reaction Sintered Mullite Ceramics, J. Manuf. Sci. Eng. 124 (2002) 875–885.

[2] F.E. Pfefferkorn, Y.C. Shin, Y. Tian, F.P. Incropera, Laser-Assisted Machining of Magnesia-Partially-Stabilized Zirconia, J. Manuf. Sci. Eng. 126 (2004) 42–

51.

[3] Z. Li, F. Zhang, X. Luo, W. Chang, Y. Cai, W. Zhong, F. Ding, Material removal mechanism of laser-assisted grinding of RB-SiC ceramics and process optimization, J. Eur. Ceram. Soc. 39 (2019) 705–717.

[4] C. Brecher, C.J. Rosen, M. Emonts, Laser-assisted milling of advanced materials, Phys. Procedia. 5 (2010) 259–272.

[5] S. Lei, Y.C. Shin, F.P. Incropera, Experimental Investigation of Thermo-Mechanical Characteristics in Laser-Assisted Machining of Silicon Nitride Ceramics, J. Manuf. Sci. Eng. 123 (2002) 639–646.

[6] J.L. Jiang, P.Q. Ge, W.B. Bi, L. Zhang, D.X. Wang, Y. Zhang, 2D/3D ground surface topography modeling considering dressing and wear effects in grinding process, Int. J. Mach. Tools Manuf. 74 (2013) 29–40.

[7] A.M. Shanawaz, S. Sundaram, U.T.S. Pillai, P. Babu Aurtherson, Grinding of aluminium silicon carbide metal matrix composite materials by electrolytic in-process dressing grinding, Int. J. Adv. Manuf. Technol. 57 (2011) 143–150.

[8] Y. Novoselov, S. Bratan, V. Bogutsky, Analysis of Relation between Grinding Wheel Wear and Abrasive Grains Wear, Procedia Eng. 150 (2016) 809–814.

[9] J. Xie, F. Wei, J.H. Zheng, J. Tamaki, A. Kubo, 3D laser investigation on micron-scale grain protrusion topography of truncated diamond grinding wheel for precision grinding performance, Int. J. Mach. Tools Manuf. 51 (2011) 411–419.

[10] D. Setti, S. Ghosh, P.V. Rao, A method for prediction of active grits count in surface grinding, Wear. 382–383 (2017) 71–77.

[11] F. Klocke, C. Wrobel, M. Rasim, P. Mattfeld, Approach of Characterization of the Grinding Wheel Topography as a Contribution to the Energy Modelling of Grinding Processes, Procedia CIRP. 46 (2016) 631–635.

[12] A. Darafon, A. Warkentin, R. Bauer, Characterization of grinding wheel topography using a white chromatic sensor, Int. J. Mach. Tools Manuf. 70 (2013) 22–31.

[13] S. Lin, Z. Jiang, Y. Yin, Research on arc-shaped wheel wear and error compensation in arc envelope grinding, Int. J. Adv. Manuf. Technol. 103 (2019) 1847-1859.

[14] M.E. Nakai, P.R. Aguiar, H. Guillardi, E.C. Bianchi, D.H. Spatti, D.M. D'Addona, Evaluation of neural models applied to the estimation of tool wear in the grinding of advanced ceramics, Expert Syst. Appl. 42 (2015) 7026–7035.

[15] F.E. Pfefferkorn, S. Lei, Y. Jeon, G. Haddad, A metric for defining the energy efficiency of thermally assisted machining, Int. J. Mach. Tools Manuf. 49 (2009) 357–365.

[16] T. Kizaki, Y. Ito, S. Tanabe, Y. Kim, N. Sugita, M. Mitsuishi, Laser-assisted Machining of Zirconia Ceramics using a Diamond Bur, Procedia CIRP. 42 (2016) 497–502.

[17] C.W. Chang, C.P. Kuo, An investigation of laser-assisted machining of Al2O3 ceramics planing, Int. J. Mach. Tools Manuf. 47 (2007) 452–461.

[18] M.J. Bermingham, S. Palanisamy, M.S. Dargusch, Understanding the tool wear mechanism during thermally assisted machining Ti-6Al-4V, Int. J. Mach. Tools

Manuf. 62 (2012) 76–87.

[19] B. Linke, F. Klocke, Temperatures and wear mechanisms in dressing of vitrified bonded grinding wheels, Int. J. Mach. Tools Manuf. 50 (2010) 552–558.

[20] W. Yang, L. Xiao, H. Chen, X. Zhang, X. Tang, Experimental study on laser power influence for diamond grits brazing, Proc. SPIE. 10964 (2018) 109646V-1–6.

[21] X. Rao, F. Zhang, X. Luo, F. Ding, Characterization of hardness, elastic modulus and fracture toughness of RB-SiC ceramics at elevated temperature by Vickers test, Mater. Sci. Eng. A. 744 (2018) 426–435.

[22] S. Clijsters, K. Liu, D. Reynaerts, B. Lauwers, EDM technology and strategy development for the manufacturing of complex parts in SiSiC, J. Mater. Process. Technol. 210 (2010) 631–641.

[23] K. Ding, Y. Fu, H. Su, X. Gong, K. Wu, Wear of diamond grinding wheel in ultrasonic vibration-assisted grinding of silicon carbide, Int. J. Adv. Manuf. Technol. 71 (2014) 1929–1938.

[24] J.Y. Shen, J.Q. Wang, B. Jiang, X.P. Xu, Study on wear of diamond wheel in ultrasonic vibration-assisted grinding ceramic, Wear. 332–333 (2015) 788–793.

[25] X. Rao, F. Zhang, X. Luo, F. Ding, Y. Cai, J. Sun, H. Liu, Material removal mode and friction behaviour of RB-SiC ceramics during scratching at elevated temperatures, J. Eur. Ceram. Soc. 39 (2019) 3534–3545.

[26] T.G. Bifano, T.A. Dow, R.O. Scattergood, Ductile-Regime Grinding: A New Technology for Machining Brittle Materials, J. Eng. Ind. 113 (1991) 184–189.

[27] Y. Quinsat, L. Sabourin, C. Lartigue, Surface topography in ball end milling process: Description of a 3D surface roughness parameter, J. Mater. Process. Technol. 195 (2008) 135–143.

[28] W.L. Chang, X.C. Luo, Q.L. Zhao, J.N. Sun, Y. Zhao, Laser Assisted Micro Grinding of High Strength Materials, Key Eng. Mater. 496 (2012) 44–49.

[29] Y.J. Lu, J. Xie, X.H. Si, Study on micro-topographical removals of diamond grain and metal bond in dry electro-contact discharge dressing of coarse diamond grinding wheel, Int. J. Mach. Tools Manuf. 88 (2015) 118–130.

[30] Y. Kang, Y. Qiu, Z. Lei, M. Hu, An application of Raman spectroscopy on the measurement of residual stress in porous silicon, Opt. Lasers Eng. 43 (2005) 847–855.

[31] Y.I. Kang, W. Qiu, Z.K. Lei, A robust method to measure residual stress in micro-structure, Optoelectron. Lett. 3 (2007) 126–128.

[32] H. Matsunami, W.S. Yoo, Solid-state phase transformation in cubic silicon carbide, Jpn. J. Appl. Phys. 30 (1991) 545–553.

[33] M. Matsumoto, H. Huang, H. Harada, K. Kakimoto, J. Yan, On the phase transformation of single-crystal 4H-SiC during nanoindentation, J. Phys. D. Appl. Phys. 50 (2017) 1–9.

[34] Z. Li, F. Zhang, Y. Zhang, X. Luo, Experimental investigation on the surface and subsurface damages characteristics and formation mechanisms in ultra-precision grinding of SiC, Int. J. Adv. Manuf. Technol. 92 (2017) 2677–2688.

[35] S. Nakashima, Y. Nakatake, Y. Ishida, T. Talkahashi, H. Okumura, Detection of

defects in SiC crystalline films by Raman, Phys. B. 308–310 (2001) 684–686.

[36] S. Nakashima, H. Harima, Raman Investigation of SiC Polytypes, Phys. Status Solidi. 1 (1997) 39–64.

[37] Y. Zhu, C. Yao, J. Wang, H. Zhu, T. Shen, X. Gao, J. Sun, K. Wei, D. Wang, Y. Sheng, Z. Wang, Micro-Raman spectroscopy characterization of silicon with different structures irradiated with energetic Bi-ions, Nucl. Instruments Methods Phys. Res. Sect. B Beam Interact. with Mater. Atoms. 365 (2015) 123–127.